ADVANCED MATERIALS
www.advmat.de

Self-Assembly of Enzyme-Like Nanofibrous G-Molecular Hydrogel for Printed Flexible Electrochemical Sensors

Ruibo Zhong, Qian Tang, Shaopeng Wang, Hongbo Zhang, Feng Zhang, Mingshu Xiao, Tiantian Man, Xiangmeng Qu, Li Li, Weijia Zhang, and Hao Pei**

Conducting hydrogels provide great potential for creating designer shape-morphing architectures for biomedical applications owing to their unique solid–liquid interface and ease of processability. Here, a novel nanofibrous hydrogel with significant enzyme-like activity that can be used as "ink" to print flexible electrochemical devices is developed. The nanofibrous hydrogel is self-assembled from guanosine (G) and $KB(OH)_4$ with simultaneous incorporation of hemin into the G-quartet scaffold, giving rise to significant enzyme-like activity. The rapid switching between the sol and gel states responsive to shear stress enables free-form fabrication of different patterns. Furthermore, the replication of the G-quartet wires into a conductive matrix by in situ catalytic deposition of polyaniline on nanofibers is demonstrated, which can be directly printed into a flexible electrochemical electrode. By loading glucose oxidase into this novel hydrogel, a flexible glucose biosensor is developed. This study sheds new light on developing artificial enzymes with new functionalities and on fabrication of flexible bioelectronics.

Flexible electronics[1] hold great promise in biomedical applications, such as artificial muscles,[2,3] epidermal sensors,[4] implantable biodevices,[5] and electronic skins.[6] Over the past decade, there has been enormous progress in the materials, device designs, and micro/nanofabrication techniques that has accelerated the development of flexible electronics. A wide range of nanomaterials and their hybrids, including 0D (metal and metal oxide nanoparticles), 1D (metal oxide nanowires, polymer nanofibers, and carbon nanotubes), and 2D (Si nanosheets, graphene, and MoS_2 nanosheets), could enable multifunctionalities and high performance without sacrificing the mechanical deformability.[7,8] For conformal integration in biological systems, it is crucial to intimately interface electronic units with internal structures of biological materials. Currently, the most extensively used fabrication strategies are thin film deposition techniques,[9,10] which directly deposit electronic units onto flexible and stretchable polymeric substrates.[11,12] However, these methods mostly result in simple planar structures and often do not satisfy the requirements for realizing bioinspired device designs with complex architectures. Moreover, beyond the primary device manufacturing challenges, biocompatibility of subcomponents is another key parameter to concern for implantable and minimally invasive applications. It is thus highly desirable to directly print electronic devices with in vitro/vivo biocompatibility into designed shapes and tailored sizes for specific applications, such as tissue engineering,[13] soft robotics,[14,15] and medical devices.[16]

The "hydrogel printing" approach may provide a suitable alternative for the fabrication of flexible electronics owing to its unique solid–liquid interface and ease of processability.[17] There have been few studies over the past years.[18–20] For example, Xing and co-workers[21] developed water-soluble elastin peptide based cryogel macroporous scaffold loading conductive polypyrrole and carbon nanotube, which could combine high elasticity, shape memory, injectability, and conductivity into a single entity. This highly flexible and resilient elastin hybrid cryogel has been demonstrated as a promising candidate for syringe-injectable biosensors and bioelectronics.

Dr. R. Zhong, Q. Tang, M. Xiao, T. Man, Dr. X. Qu, Prof. L. Li, Prof. H. Pei
Shanghai Key Laboratory of Green Chemistry and Chemical Processes
School of Chemistry and Molecular Engineering
East China Normal University
500 Dongchuan Road
Shanghai 200241, P. R. China
E-mail: peihao@chem.ecnu.edu.cn

Dr. S. Wang
Division of Physical Biology and Bioimaging Center College of Life Sciences
Shanghai Institute of Applied Physics
Chinese Academy of Sciences
Shanghai 201800, P. R. China

The ORCID identification number(s) for the author(s) of this article can be found under https://doi.org/10.1002/adma.201706887.

DOI: 10.1002/adma.201706887

Prof. H. Zhang
Department of Pharmaceutical Science
Åbo Akademic University
FI-20520 Turku, Finland

Prof. F. Zhang
Department of Biomedical Engineering
School of Basic Medical Sciences
Guangzhou Medical University
Guangzhou 511436, P. R. China
E-mail: fengzhang1978@hotmail.com, fengzhang1978@imau.edu.cn

Prof. W. Zhang
Institutes of Biomedical Sciences and Zhongshan Hospital
Fudan University
Shanghai 200032, P. R. China

In this work, we developed a novel nanofibrous hydrogel with significant enzyme-like activity that can be used as "ink" to print flexible bioelectronic devices. This nanofibrous hydrogel was self-assembled from guanosine (G) and 0.5 equiv. of $KB(OH)_4$ that involves the cation-templated formation of G-quartet motifs and ensuing stacking into G-quartet wires.[22–25] The simultaneous incorporation of hemin into G-quartet scaffold during the self-assembly process yielded an enzyme-like nanofibrous hydrogel.[26] The rapid switching between the sol and gel states responsive to shear stress enables free-form fabrication of different patterns.[27] Moreover, we demonstrated the replication of the G-quartet wires into conductive matrix by in situ catalytic deposition of polyaniline (PANI) on nanofibers.[28] Given the shape-morphing capability, this conductive hybrid hydrogel shows great promise for applications in flexible bioelectronics. We demonstrated this concept by directly inject printing an electrochemical electrode, which is useful for developing a flexible glucose biosensor by loading glucose oxidase (GOx).[29–32]

As illustrated in **Figure 1**a, G-boronate diester is initially formed from reaction between 100×10^{-3} M G and 0.5 equiv. of $B(OH)_3$.[22] The addition of K^+ ions facilitates the cation-templated assembly of G-quartet motif, which then acts as the key building block for constructing the nanofibrous hydrogel network. Stacking of these G-quartets into columnar structures combined with the simultaneous incorporation of hemin gives rise to the enzyme-like nanofibrous hydrogel (termed H/G4 hydrogel).[33] Here, boronate ester plays an important role in stabilizing the hydrogel.[34–37] On the one hand, boric acid forming ester with G increases the solubility of G; on the other hand, boric acid connecting G in the vertical direction forms nanofibers and further forms a hydrogel.[22–24] Such a cation-templated formation and stacking of G-quartet motifs was confirmed by circular dichroism (CD) spectroscopy (Figure S1, Supporting Information), and the fibrous structures of H/G4 hydrogel with a diameter of 2 ± 0.2 nm was confirmed by atomic force microscopy (AFM) image (Figure 1; Figure S4, Supporting Information). The incorporation of hemin endows the resulting nanofibrous hydrogel peroxidase-mimicking activity. By using the H_2O_2/tetramethyl benzidine (TMB) oxidation as a model reaction, we examined the enzymatic activity of hydrogels and found that the incorporation of hemin into the nanofibrous scaffold significantly enhanced the catalytic activity compared with the free hemin (sixfold decrease in K_M, tenfold increase in k_{cat}, Figure 1b).

To quantitatively assess the mechanical properties of hydrogels, we then carried out rheological measurements performed with hydrogels containing 100×10^{-3} M guanosine and 0.5 equiv. $KB(OH)_4$. Dynamic frequency sweeps were performed for both G4 hydrogel and H/G4 hydrogel with a fixed stress of 1 Pa. As shown in **Figure 2**a, the dynamic frequency sweeps of both hydrogels showed a wide linear viscoelastic region, and the storage modulus (G') was higher than the loss modulus (G'') in each case, which verified the hydrogel formation. In addition, the G' was $\approx 10^3$ Pa in each case, suggesting that both were strong hydrogels, which is consistent with previous report.[38,39] The stress sweeps were also conducted for both hydrogels with a fixed frequency of 1 rad s^{-1} from 1 to 100 Pa. As shown in Figure 2b, both G' and G'' remained constant in the low shear stress region (stress ≤ 10 Pa); however G' rapidly decreased

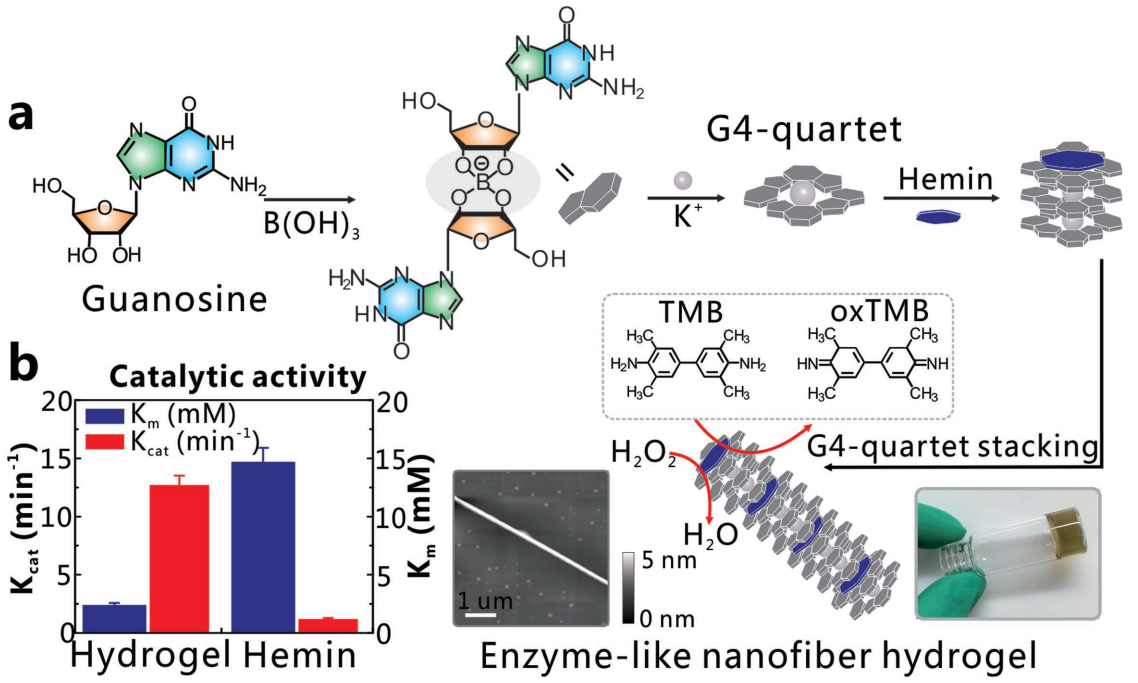

Figure 1. a) The H/G4 hydrogel is self-assembled from G and $B(OH)_3$, via formation of K^+-templated G4-quartet, followed by the stacking of G4-quartets and the simultaneous incorporation of hemin to give rise to enzyme-like nanofibrous hydrogel. The inset photograph shows a tilted vial containing brown colored H/G4 hydrogel. The inset AFM image shows an H/G4 hydrogel fiber with a diameter of 2 ± 0.2 nm. b) Comparison of catalytic activity between H/G4 hydrogel and free hemin.

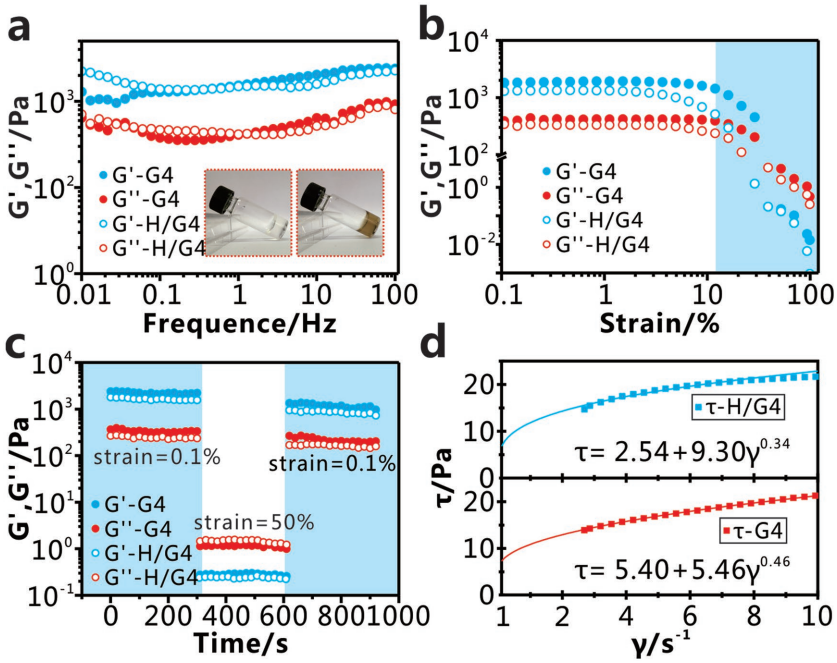

Figure 2. Rheological properties and characterization of both G4 hydrogel and H/G4 hydrogel and their direct writable behavior. a) Rheological frequency sweeps of G4 hydrogel and H/G4 hydrogel with a fixed stress of 1 Pa, respectively. The inset photographs show the tilted vials containing G4 hydrogel (left) and H/G4 hydrogel (right), respectively. b) Rheological stress sweeps of G4 hydrogel (100×10^{-3} M guanosine and 0.5 equiv. $KB(OH)_4$) and H/G4 hydrogel (100×10^{-6} M hemin) with a fixed frequency of 1 rad s^{-1}. c) Step strain measurements of G4 hydrogel and H/G4 hydrogel with a fixed frequency of 1 rad s^{-1}. Each strain interval was kept as 5 min. d) Flow curves of shear stress measured as a function of the applied shear rate for G4 hydrogel and H/G4 hydrogel. The data can be well fitted by the Herschel–Bulkley model ($\tau = \tau_0 + K\dot{\gamma}^n$, where τ is the shear stress (Pa), $\dot{\gamma}$ is the shear rate (s^{-1}), τ_0 is the yield stress (Pa), K is the consistency coefficient (Pa s^n), and n is the flow behavior index). Both H/G4 hydrogel and G4 hydrogel were prepared with G (100×10^{-3} M) and $B(OH)_3$ (50×10^{-3} M). The concentrations of K^+ and hemin were 50×10^{-3} and 100×10^{-6} M, respectively. All experiments were conducted at 25 °C.

after the shear stress exceeded ≈10 Pa, indicating a gel-to-sol transition. We also performed step strain measurements to investigate their thixotropic behavior. Under a 0.1% strain, G' was larger than G'', indicating that both formed self-standing hydrogels. As the strain stepped to 50%, G' and G'' were inverted, resulting in a quasiliquid state, while they immediately recovered to 90% of their initial states after the strain back to 0.1%. More interestingly, the rapid switching between the sol and gel states by varying the shear stress allows direct 3D printing, in which the sol state ensures the components going through a needle easily, and the fast mechanical strength recovering at low shear stress allows the rapid shaping of injection. For instance, as shown in Figure S2 (Supporting Information), the H/G4 hydrogel can be used as "ink" which can be directly written into a 3D star-shaped pattern on a poly(dimethylsiloxane) (PDMS) substrate via a 1 mL syringe "pen." Moreover, from the ascending flow curves of shear stress measured as a function of the applied shear rate (Figure 2d), we can observe that both hydrogels exhibited a non-Newtonian pseudoplastic behavior.[40] The data can be accurately fitted by the Herschel–Bulkley model.[41] Specifically, the flow behavior index of H/G4 hydrogel ($n = 0.34$) is slightly smaller than that of G4 hydrogel ($n = 0.46$), indicating that the incorporation of hemin into the G4 network had no obvious influence on the rheology properties. The yield stress of H/G4 hydrogel (2.54 Pa) was reduced half than that of G4 hydrogel (5.40 Pa), indicating that less energy is needed to initiate the flow. Taken together, these results demonstrated that both G4 hydrogel and H/G4 hydrogel have excellent thixotropic properties, and the incorporation of hemin did not alter the mechanical properties of hydrogel given their similar rheological behaviors.

The incorporation of hemin into the G4-quartet endows the resulting H/G4 hydrogel peroxidase-mimicking activity. By using the H_2O_2/TMB oxidation as a model reaction, we examined the enzymatic activity of hydrogels in different forms. We first interrogated the effect of different G/hemin molar ratios on the enzymatic activity of the resulting H/G4 hydrogel. We measured this using a peroxidase-type colorimetric assay by the hemin-catalyzed oxidation of chromogenic substrate (TMB) into colored products in the presences of H_2O_2.[42,43] **Figure 3**a displays the Michaelis–Menten plots for initial peroxidation rate as a function of H_2O_2 concentration for H/G4 hydrogels fabricated with G/hemin molar ratios of 12:1 and 4:1. The Michaelis–Menten constants[33,44] (K_M) of the 12:1 ratio is similar to that of G4–DNA (Figure 3a and **Table 1**), suggesting that a ratio of 12:1 gives rise to an enzyme-mimicking hydrogel. In addition, the incorporation of hemin into the nanofibrous scaffold significantly enhanced the catalytic activity, in which the turnover number (k_{cat}) of free hemin (1.2 ± 0.10) increased tenfold (to 12.72 ± 0.80) for the 12:1 ratio. Given the important role of K^+ involved in the templation of G4-quartet motifs, we next evaluated the effect of different K^+/G molar ratios ($n = K^+/G = 0.25$, 0.5, 1.0, or 2.0). As shown in Figure 3b and Table 1, the H/G4 hydrogels fabricated with different K^+/G molar ratios exhibited similar K_M toward H_2O_2/TMB oxidation; however, the addition of 0.5 equiv. of K^+ relative to the concentration of G gave rise to slightly higher k_{cat} compared to other molar ratios, thus the optimal K^+/G molar ratio was determined as 0.5 for future experiments. We next sought to quantify the cation's influence by comparing the enzymatic activity of the resulting H/G4 hydrogel. As shown in Figure S3 (Supporting Information), only K^+ and Na^+ systems can form hydrogels, and the K^+–H/G4 hydrogel exhibited the highest enzyme efficiency, with a 66-fold increase compared to free hemin and 2–5-fold increase compared to other cations.[45,46]

Having established the optimal synthetic parameters for the H/G4 hydrogel, we next sought to apply its enzyme-mimicking function in the fabrication of nanofibrous structured conductive material. As schematically illustrated in **Figure 4**a, the H/G4 hydrogel acts as a catalytic matrix that catalyzes the oxidation

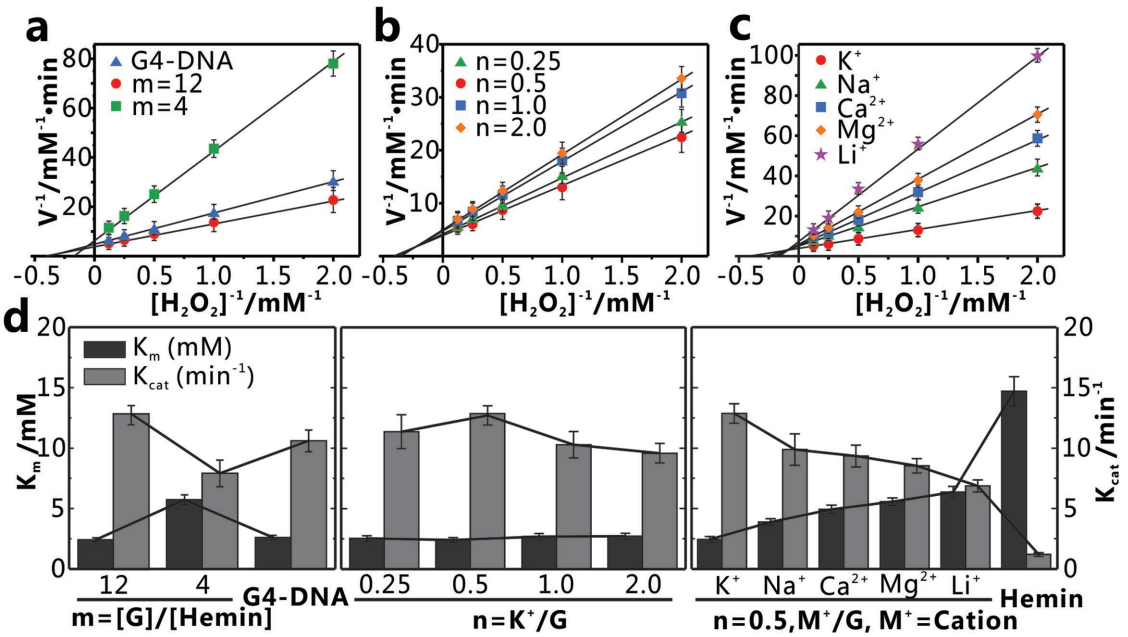

Figure 3. Characterization of enzymatic activity of H/G4 hydrogels in different forms using the H_2O_2/TMB oxidation as a model reaction. a) The effect of different G/hemin molar ratios (m = G/hemin = 12:1 or 4:1, compared to G4–DNA as a reference) on the initial peroxidation rates of the resulting H/G4 hydrogels. b) The effect of different K^+/G molar ratios (n = K^+/G = 0.25, 0.5, 1.0, or 2.0) on the initial peroxidation rates of the resulting H/G4 hydrogels. c) The effect of different stabilizing metal cations (R^+ = cation = K^+, Na^+, Ca^{2+}, Mg^{2+}, or Li^+, n = R^+/G = 0.5) on the initial peroxidation rates of the resulting H/G4 hydrogels. d) Comparison of K_M and k_{cat} for free hemin, G4–DNA, and H/G4 hydrogels in different forms.

of aniline by H_2O_2 to PANI.[47,48] The deposition of PANI onto the nanofibrous hydrogel scaffold was conducted in the presence of aniline/H_2O_2, pH = 3.0, for 3 h. It should be noted that the original H/G4 hydrogel was not very stable at pH = 3.0, we thus mixed 1% agarose in the H/G4 hydrogel to improve its stability. The resulting hybrid hydrogel replicated the interconnected nanofibrous structure, yielding ≈2 nm thick PANI coating as confirmed by AFM characterization (Figure S4, Supporting Information). The resulting PANI-functionalized hydrogels were then subjected to pH = 8 to form a brown-colored, proton-undoped hydrogel (middle panel in Figure 4a), or treated with 2 M HCl to yield a dark green-colored, proton-doped hydrogel (right panel in Figure 4a).[49–52] We then examined the electrochemical properties of both proton-undoped and doped H/G4–PANI hydrogels on an indium tin oxide (ITO) substrate using cyclic voltammetry (CV), scanning in between –0.4 and 0.4 V at a scan rate of 100 mV s^{-1}. As shown in Figure 4b, at pH = 8, the H/G4–PANI hydrogel displayed a quasireversible CV wave at ≈ –0.05 V versus Ag/AgCl, corresponding to a proton-undoped configuration of PANI; at pH = 3, CV characteristic of proton-doped PANI was observed, indicating enhanced electrochemical properties of a conducting PANI state. We further evaluated the conductivities of the H/G4–PANI hydrogels at both proton-undoped and doped states. As depicted in Figure 4c, the proton-undoped H/G4–PANI hydrogel showed the I–V curve characteristic of an insulating material, suggesting the very high resistance of the polymer matrix without proton doping, whereas the proton-doped H/G4–PANI hydrogel showed the I–V curve characteristic of a conducting material, indicating that the proton doping resulted in the formation of an electrically conducting polymer matrix. This chemical transition of PANI from the insulating base state to the conducting salt state upon proton doping was also verified by the absorption spectra (Figure 4d). Specifically, an absorbance band at ≈460 nm at proton-undoped state (pH = 8) is redshifted to ≈750 nm at proton-doped state (pH = 3), consistent with the color change from brown to dark green as shown in the middle and right panels in Figure 4a.

The unique 3D printing feature and electrical properties of H/G4–PANI hydrogel make it attractive building block for electronic applications, such as glucose sensors and self-regulated insulin delivery devices.[53–57] As a proof of concept,

Table 1. K_M, k_{cat}, and enzyme efficiency of free hemin, G4–DNA, and H/G4 hydrogels in different forms.

	K_M [×10^{-3} M]	k_{cat} [min^{-1}]	K_M/k_{cat} [m M min^{-1}]
Hemin	14.70 ± 1.20	1.20 ± 0.10	0.08 ± 0.01
G4–DNA	2.60 ± 0.12	10.6 ± 0.90	4.08 ± 0.57
m = 4	5.73 ± 0.41	7.91 ± 1.10	1.38 ± 0.29
m = 12	2.41 ± 0.17	12.72 ± 0.80	5.28 ± 0.71
n = 0.25	2.54 ± 0.23	11.37 ± 1.40	4.48 ± 0.96
n = 0.5	2.41 ± 0.17	12.72 ± 0.80	5.28 ± 0.71
n = 1.0	2.69 ± 0.26	10.29 ± 1.10	3.83 ± 0.79
n = 2.0	2.72 ± 0.24	9.59 ± 0.80	3.53 ± 0.61
n = 0.5, Na^+	3.88 ± 0.28	9.87 ± 1.30	2.54 ± 0.52
n = 0.5, Ca^{2+}	4.93 ± 0.35	9.33 ± 0.90	1.89 ± 0.32
n = 0.5, Mg^{2+}	5.56 ± 0.31	8.52 ± 0.60	1.53 ± 0.19
n = 0.5, Li^+	6.36 ± 0.47	6.86 ± 0.50	1.08 ± 0.16

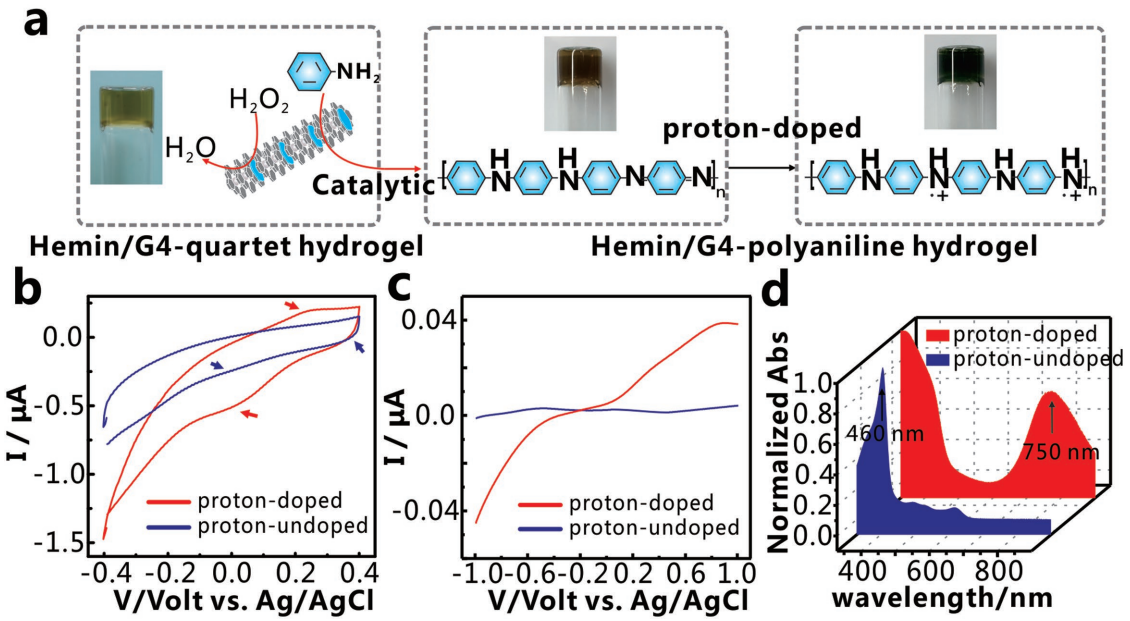

Figure 4. a) Schematic illustrating the fabrication of H/G4–PANI hydrogel by applying H/G4 hydrogel as a catalytic matrix for the deposition of PANI. Inset photographs from left to right panels: H/G4 hydrogel, proton-undoped H/G4–PANI hydrogel (pH = 8), and proton-doped H/G4–PANI hydrogel (pH = 3). b) CV of both proton-undoped and doped H/G4–PANI hydrogels on an ITO substrate. The voltammograms were recorded in a 1×10^{-3} M $K_3[Fe(CN)_6] + 0.5$ M KNO_3 aqueous electrolyte at a scan rate of 100 mV s^{-1}; Ag/AgCl reference electrode and Pt mesh counterelectrode were employed. c) *I–V* curves of the proton-undoped and doped H/G4–PANI hydrogels. d) Absorption spectra of the proton-undoped and doped H/G4–PANI hydrogels.

we fabricated a glucose biosensor by loading glucose oxidase enzyme into our H/G4–PANI hydrogel (**Figure 5**a,b). The electrochemical properties of H/G4–PANI hydrogel showed no significant changes before (red line) and after GOx loading (blue line). It is likely because that the GOx being loaded in the micropores of the hydrogel, thus not affecting the conductivity of H/G4–PANI hydrogel (Figure S5, Supporting Information). We first investigated the enzymatic properties of proton-doped H/G4–PANI hydrogel toward H_2O_2 reduction. The electrochemical signal is highly responsive to different concentrations of H_2O_2 (Figure S6, Supporting Information), which showed the linear correlation between the cathodic peak current at −0.4 V and the concentration of H_2O_2 over the (1–10) $\times 10^{-3}$ M range. The electrocatalytic cathodic currents were monotonically increased using the GOx-loaded H/G4–PANI hydrogel for the reduction of the GOx-generated H_2O_2 (Figure 5c), making it a high promising flexible material for glucose sensors. Moreover, the GOx-loaded H/G4–PANI hydrogel exhibited good long-term stability. After stored at 4 °C for one week, the conductivity of GOx-loaded H/G4–PANI hydrogel only showed a minor decrease (Figure S7a, Supporting Information). Nevertheless, the GOx-loaded H/G4–PANI hydrogel still demonstrated good long-term stability, exhibiting no degradation of sensing performance after 100 cycles (Figure S7b, Supporting Information). The H/G4–PANI hydrogel film exhibited excellent electrochemical and electrochromic properties, which turned from the pale yellow reduced state to green oxidized state with increasing potentials from −0.2 to +1.3 V (Figure 5c). The electrochemical stability of the H/G4–PANI hydrogel film was further investigated by switching potentials with a 4 s delay at each state (Figure 5d), which exhibited good cycle stability with no obvious current drop after five cycles. These results demonstrated that the H/G4–PANI hydrogel provides a promising material for flexible electrochemical applications.[58,59]

In summary, we have developed an enzyme-like nanofibrous hydrogel by simultaneously incorporating hemin into G-quartet scaffold during the cation-templated self-assembly between G and $KB(OH)_4$, and further applied its enzyme-mimicking function in the fabrication of semiconducting H/G4–PANI hydrogel for flexible electrochemical sensors. This nanofabrication strategy provides several unprecedented advantages that makes it a promising method for developing artificial enzymes and next-generation flexible bioelectronics. First, the coassembly of cationic hemin with anionic borate esters enables the well-defined arrangement of catalytic active sites during the stacking of G-quartets to ultimately form a nanofibrous hydrogel matrix, which endows the resulting H/G4 hydrogel efficient enzyme-like property. This self-assembly approach therefore provides a promising method for developing hydrogels to mimic natural enzymes. Second, this enzyme-like H/G4 hydrogel can be employed as a catalytic matrix for in situ formation of semiconducting nanofibrous H/G4–PANI hydrogel network, which has been demonstrated as an excellent building block to construct nanodevices. Finally, given the biological nature of hydrogel components and its direct printing capability, our nanofabrication strategy provides great potential for sophisticated engineering of hierarchical architecture performing complex bioelectronic function. Therefore, we expect this enzyme-like nanofibrous semiconducting hydrogel to hold great promise for developing artificial enzymes with new functionalities, and our nanofabrication strategy might open up new possibilities for creating designer shape-morphing architectures for future bioelectronic applications.

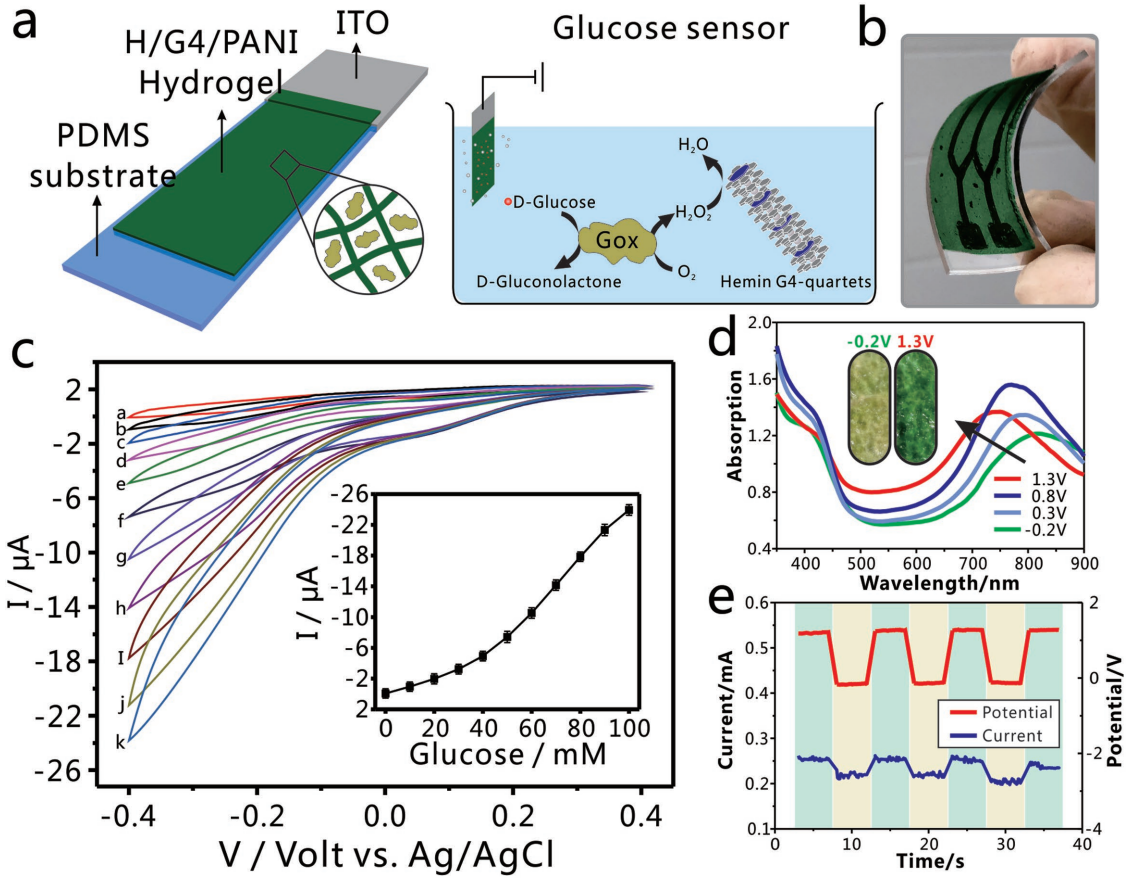

Figure 5. a) Scheme of the glucose sensor based on GOx-loaded H/G4–PANI hydrogel for the detection of glucose. b) The optical image of the glucose sensor. c) Cyclic volatammograms of glucose sensor in the presence of different concentrations of glucose. Inset indicates the linear correlation of cathodic peak current at –0.4 V with the concentration of glucose. d) UV–vis absorption spectra of the H/G4–PANI hydrogel film measured at different potentials (–0.2 to +1.3 V with a step size of 0.5 V) in an 0.25 M HCl solution. Inset: photographic images of the H/G4–PANI hydrogel film at different applied potentials. e) Potential and chronoamperometry curves of the H/G4–PANI hydrogel film.

Experimental Section

Materials: Guanosine and hemin were purchased from BBI Life Sciences, Sangon, Shanghai. Agarose was purchased from Biowest, Spain. Other reagents were purchased from Aladin, Shanghai. All the reagents were used directly with no further purification. The ssDNA (TTTTGGGTTGGGCGGGATGGGTTTT) for assembling hemin/G-quadruplex and DNAzyme was purchased from Sangon, Shanghai.

Instruments: The UV–vis absorption spectra were acquired using an Agilent Carry 60 spectrophotometer. Scanning electron microscope imaging was performed on a Hitachi S-4800 microscope. The electrochemical properties of the hydrogel were characterized using Autolab PGSTAT302N (Metrohm, Swiss). The atomic force microscopy imaging was carried out using the automode on a silicon wafer under air condition with a multimode-8 controller from Bruker Instruments. The circular dichroism spectra for a 2 wt% H/G4 hydrogel were recorded at room temperature on a Jasco J-815 CD spectrometer.

Preparation of H/G4 Hydrogel and G4–DNA: The desired amount of G (100×10^{-3} M) was weighed into a vial, followed by the addition of the appropriate amount of $B(OH)_3$ solution to reach a final concentration of 50×10^{-3} M (and water if necessary). The mixture was sonicated for ≈30 s, and then the appropriate amount of KOH solution to reach a final concentration of 50×10^{-3} M was added, followed by the heat treatment at 95 °C in a water bath until G was dissolved and the solution was clear. The resulting solution was then allowed to cool to ≈60 °C, followed by the addition of hemin to reach a final concentration of 100×10^{-6} M. The hydrogel was aged at room temperature for 2 h before use in order to stabilize the formation of H/G4 hydrogel structure. Unless otherwise noted, hydrogels were prepared at a 2:1 ratio of G:$KB(OH)_4$.

Preparation of G4–DNA by a Standard Procedure: 200×10^{-6} M ssDNA solution (10×10^{-3} M N-2-hydroxyethylpiperazine-N′-2-ethanesulfonic acid (HEPES)–NH_4OH, pH = 8.0, containing 20×10^{-3} M KCl and 200×10^{-3} M NaCl) was heated at 95 °C for 5 min and then cooled to room temperature, followed by the addition of hemin to reach a final concentration of 100×10^{-6} M. The mixture solution was kept at room temperature for 2 h to allow the formation of G4–DNA.

Characterization of Enzymatic Activity: 400 µL H_2O_2/TMB substrate solution was mixed with 100 µL as-prepared H/G4 hydrogel or G4–DNA. To characterize the oxidation rate of TMB, the absorbance at 652 nm was monitored by a microplate reader (Cary 60 UV–vis spectrometer, Aglient). The kinetic parameters were calculated from the initial reaction rate V at varying concentrations of H_2O_2 (1, 2, 4, 6, and 8×10^{-3} M, respectively) based on the Lineweaver–Burk plot, $1/V = K_m/(V_{max} \times [S]) + 1/V_{max}$, where the initial reaction rate V is determined from the changes in absorbance during the first 60 s, K_m is the Michaelis constant (the substrate concentration at which the reaction rate is at half-maximum and an inverse measure of the substrate's affinity for enzyme), V_{max} is the maximum reaction rate, and $[S]$ is the substrate concentration. ε of TMB is 39 000 M^{-1} cm^{-1}. $K_{cat} = V_{max}/[\text{Enzyme}]$, where K_{cat} is the turnover number (the maximum number of substrate molecules converted to produce per enzyme molecule per second).

Preparation of Agarose-Mixed H/G4–Polyaniline (H/G4–PANI) Hydrogel: The H/G4 hydrogel was synthesized following the protocol previously described. The only difference was the addition of 1% agarose at the heating step. The resulting solution was allowed to cool to ≈60 °C, followed by the addition of hemin to reach a final concentration of 100×10^{-6} M. The hydrogel was aged at room temperature for 2 h before use in order to stabilize the formation of H/G4 hydrogel structure. Then, the hydrogel was transferred into a 50×10^{-3} M aniline solution (10×10^{-3} M HEPES–HCl buffer, pH = 3.0) for 2 h. H_2O_2 was subsequently (final concentration of 50×10^{-3} M) added to the aniline/hydrogel system to initiate the aniline polymerization for 1 h.

Preparation of GOx-Loaded H/G4–PANI Hydrogel: First, emerge the previously prepared H/G4–PANI hydrogel into the HEPES buffer solution (10×10^{-3} M, pH 7.4, KCl 50×10^{-3} M) for 1 h to change the acidic hydrogel into neutral. Then, transfer the hydrogel into the HEPES buffer solution (10×10^{-3} M, pH 7.4, KCl 50×10^{-3} M) containing 1 mg mL^{-1} GOx for 1 h to load the GOx into the hydrogel.

Fabrication and Characterization of the Electrochromic Electrode: The ITO substrate was rinsed with acetone, ethanol, and deionized water in sequence to remove contaminants from the surface. The cleansed ITO glass was then dried and used as the substrate for the H/G4–PANI hydrogel film. The electrochromic electrode was fabricated by directly inject printing the H/G4–PANI hydrogel onto the ITO glass with an area of 2 cm^2 (1 cm × 2 cm) and a thickness of ≈1 mm, followed by drying at 60 °C for 3 min.

The electrochromic properties of the H/G4–PANI hydrogel were characterized by using a PGSTAT128N Potentiostat with a three-electrode system, which consisted of the H/G4–PANI hydrogel coated ITO glass as the working electrode, platinum as the counterelectrode, and Ag/AgCl as the reference electrode. A 0.25 M HCl solution was used as the electrolyte.

Supporting Information

Supporting Information is available from the Wiley Online Library or from the author.

Acknowledgements

R.Z., Q.T., and S.W. contributed equally to this work. This work was supported by the National Science Foundation of China (Grant Nos. 21722502, 21505045, 21705048, and 51763019), the Shanghai Pujiang Talent Project (Grant Nos. 16PJ1402700 and 15PJ1401800), China Postdoctoral Science Foundation (Grant Nos. 2015M581565 and 2017T100283), STCSM 17JC1400200, and Jane and Aatos Erkko Foundation (Grant No. 4704010).

Conflict of Interest

The authors declare no conflict of interest.

Keywords

enzyme mimicking, flexible electrochemical sensors, guanosine, low-molecular-weight hydrogels, self-assembly

Received: November 24, 2017
Published online: February 1, 2018

[1] J. A. Rogers, T. Someya, Y. Huang, *Science* **2010**, *327*, 1603.
[2] H. Stoyanov, M. Kollosche, S. Risse, R. Waché, G. Kofod, *Adv. Mater.* **2013**, *25*, 578.
[3] B. Tian, J. Liu, T. Dvir, L. Jin, J. H. Tsui, Q. Qing, Z. Suo, R. Langer, D. S. Kohane, C. M. Lieber, *Nat. Mater.* **2012**, *11*, 986.
[4] D.-H. Kim, N. Lu, R. Ma, Y.-S. Kim, R.-H. Kim, S. Wang, J. Wu, S. M. Won, H. Tao, A. Islam, K. J. Yu, T.-I. Kim, R. Chowdhury, M. Ying, L. Xu, M. Li, H.-J. Chung, H. Keum, M. McCormick, P. Liu, Y.-W. Zhang, F. G. Omenetto, Y. Huang, T. Coleman, J. A. Rogers, *Science* **2011**, *333*, 838.
[5] D.-H. Kim, J. Viventi, J. J. Amsden, J. Xiao, L. Vigeland, Y.-S. Kim, J. A. Blanco, B. Panilaitis, E. S. Frechette, D. Contreras, D. L. Kaplan, F. G. Omenetto, Y. Huang, K.-C. Hwang, M. R. Zakin, B. Litt, J. A. Rogers, *Nat. Mater.* **2010**, *9*, 511.
[6] C. Wang, D. Hwang, Z. Yu, K. Takei, J. Park, T. Chen, B. Ma, A. Javey, *Nat. Mater.* **2013**, *12*, 899.
[7] S. Choi, H. Lee, R. Ghaffari, T. Hyeon, D.-H. Kim, *Adv. Mater.* **2016**, *28*, 4203.
[8] Y. Lee, J. Kim, H. Joo, M. S. Raj, R. Ghaffari, D.-H. Kim, *Adv. Mater. Technol.* **2017**, *2*, 1700053.
[9] L. Li, U. Steiner, S. Mahajan, *J. Mater. Chem.* **2010**, *20*, 7131.
[10] M. R. J. Scherer, L. Li, P. M. S. Cunha, O. A. Scherman, U. Steiner, *Adv. Mater.* **2012**, *24*, 1217
[11] A. M. Coclite, R. M. Howden, D. C. Borrelli, C. D. Petruczok, R. Yang, J. L. Yagüe, A. Ugur, N. Chen, S. Lee, W. J. Jo, A. Liu, X. Wang, K. K. Gleason, *Adv. Mater.* **2013**, *25*, 5392.
[12] S. I. Park, D. S. Brenner, G. Shin, C. D. Morgan, B. A. Copits, H. U. Chung, M. Y. Pullen, K. N. Noh, S. Davidson, S. J. Oh, J. Yoon, K.-I. Jang, V. K. Samineni, M. Norman, J. G. Grajales-Reyes, S. K. Vogt, S. S. Sundaram, K. M. Wilson, J. S. Ha, R. Xu, T. Pan, T.-I. Kim, Y. Huang, M. C. Montana, J. P. Golden, M. R. Bruchas, R. W. Gereau, J. A. Rogers, *Nat. Biotechnol.* **2015**, *33*, 1280.
[13] G. Park, H.-J. Chung, K. Kim, S. Lim, J. Kim, Y.-S. Kim, Y. Liu, W.-H. Yeo, R.-H. Kim, S. S. Kim, J.-S. Kim, Y. H. Jung, T.-I. Kim, C. Yee, J. A. Rogers, K.-M. Lee, *Adv. Healthcare Mater.* **2014**, *3*, 515.
[14] D. Rus, M. T. Tolley, *Nature* **2015**, *521*, 467.
[15] N. Lu, D.-H. Kim, *Soft Rob.* **2014**, *1*, 53.
[16] J. Viventi, D.-H. Kim, J. D. Moss, Y.-S. Kim, J. A. Blanco, N. Annetta, A. Hicks, J. Xiao, Y. Huang, D. J. Callans, J. A. Rogers, B. Litt, *Sci. Trans. Med.* **2010**, *2*, 24ra22.
[17] J. Malda, J. Visser, F. P. Melchels, T. Jüngst, W. E. Hennink, W. J. A. Dhert, J. Groll, D. W. Hutmacher, *Adv. Mater.* **2013**, *25*, 5011.
[18] J. S. Kahn, A. Trifonov, A. Cecconello, W. Guo, C. Fan, I. Willner, *Nano Lett.* **2015**, *15*, 7773.
[19] P. Song, D. Ye, X. Zuo, J. Li, J. Wang, H. Liu, M. T. Hwang, J. Chao, S. Su, L. Wang, J. Shi, L. Wang, W. Huang, R. Lal, C. Fan, *Nano Lett.17*, **2017**, 5193.
[20] J. Wang, J. Chao, H. Liu, S. Su, L. Wang, W. Huang, I. Willner, C. Fan, *Angew. Chem., Int. Ed.* **2017**, *56*, 2171.
[21] Y. Liu, K. Xu, Q. Chang, M. A. Darabi, B. Lin, W. Zhong, M. Xing, *Adv. Mater.* **2016**, *28*, 7758.
[22] G. M. Peters, L. P. Skala, T. N. Plank, B. J. Hyman, G. N. Manjunatha Reddy, A. Marsh, S. P. Brown, J. T. Davis, *J. Am. Chem. Soc.* **2014**, *136*, 12596.
[23] G. M. Peters, L. P. Skala, J. T. Davis, *J. Am. Chem. Soc.* **2016**, *138*, 134.
[24] G. M. Peters, L. P. Skala, T. N. Plank, H. Oh, G. N. Manjunatha Reddy, A. Marsh, S. P. Brown, S. R. Raghavan, J. T. Davis, *J. Am. Chem. Soc.* **2015**, *137*, 5819.
[25] V. Venkatesh, N. K. Mishra, I. Romero-Canelón, R. R. Vernooij, H. Shi, J. P. C. Coverdale, A. Habtemariam, S. Verma, P. J. Sadler, *J. Am. Chem. Soc.* **2017**, *139*, 5656.
[26] T. Bhattacharyya, Y. P. Kumar, J. Dash, *ACS Biomater. Sci. Eng.* **2017**, *3*, 2358.
[27] M. R. J. Scherer, U. Steiner, *Nano Lett.* **2013**, *13*, 3005.
[28] A. G. Macdiarmid, J. C. Chiang, A. F. Richter, A. J. Epstein, *Synth. Met.* **1987**, *18*, 285.
[29] A. Zhang, C. M. Lieber, *Chem. Rev.* **2016**, *116*, 215.

[30] Y. Ma, K.-I. Jang, L. Wang, H. N. Jung, J. W. Kwak, Y. Xue, H. Chen, Y. Yang, D. Shi, X. Feng, J. A. Rogers, Y. Huang, *Adv. Funct. Mater.* **2016**, *26*, 5345.
[31] J. A. Fan, W. H. Yeo, Y. Su, Y. Hattori, W. Lee, S. Y. Jung, Y. Zhang, Z. Liu, H. Cheng, L. Falgout, M. Bajema, T. Coleman, D. Gregoire, R. J. Larsen, Y. Huang, J. A. Rogers, *Nat. Commun.* **2014**, *5*, 3266.
[32] G. Schwartz, B. C.-K. Tee, J. Mei, A. L. Appleton, D. H. Kim, H. Wang, Z. Bao, *Nat. Commun.* **2013**, *4*, 1859.
[33] P. Travascio, Y. Li, D. Sen, *Chem. Biol.* **1998**, *5*, 505.
[34] Y. Guan, Y. Zhang, *Chem. Soc. Rev.* **2013**, *42*, 8106.
[35] N. Sreenivasachary, J.-M. Lehn, *Chem. – Asian J.* **2008**, *3*, 134.
[36] T. N. Plank, J. T. Davis, *Chem. Commun.* **2016**, *52*, 5037.
[37] L. E. Buerkle, Z. Li, A. M. Jamieson, S. J. Rowan, *Langmuir* **2009**, *25*, 8833.
[38] C. Li, A. Faulkner-Jones, A. R. Dun, J. Jin, P. Chen, Y. Xing, Z. Yang, Z. Li, W. Shu, D. Liu, R. R. Duncan, *Angew. Chem., Int. Ed.* **2015**, *54*, 3957.
[39] C. Li, P. Chen, Y. Shao, X. Zhou, Y. Wu, Z. Yang, Z. Li, T. Weil, D. Liu, *Small* **2015**, *11*, 1138
[40] G. Astarita, G. Marrucci, *Principles of Non-Newtonian Fluid Mechanics*. McGraw-Hill Companies, New York **1974**.
[41] W. H. Herschel, R. Bulkley, *Kolloid-Z.* **1926**, *39*, 291.
[42] B. Li, Y. Du, T. Li, S. Dong, *Anal. Chim. Acta* **2009**, *651*, 234.
[43] P. D. Josephy, T. Eling, R. P. Mason, *J. Biol. Chem.* **1982**, *257*, 3669.
[44] X. Mao, A. J. Simon, H. Pei, J. Shi, J. Li, Q. Huang, K. W. Plaxco, C. Fan, *Chem. Sci.* **2016**, *7*, 1200.
[45] W. Li, Y. Li, Z. Liu, B. Lin, H. Yi, F. Xu, Z. Nie, S. Yao, *Nucl. Acids Res.* **2016**, *44*, 7373.
[46] D. Bhattacharyya, G. Mirihana Arachchilage, S. Basu, *Front. Chem.* **2016**, *4*, 38.
[47] C.-H. Lu, W. Guo, X.-J. Qi, A. Neubauer, Y. Paltiel, I. Willner, *Chem. Sci.* **2015**, *6*, 6659.
[48] S. P. Surwade, S. R. Agnihotra, V. Dua, N. Manohar, S. Jain, S. Ammu, S. K. Manohar, *J. Am. Chem. Soc.* **2009**, *131*, 12528.
[49] W. E. Rudzinski, *J. Electrochem. Soc.* **1990**, *137*, 3132.
[50] R. Prakash, *J. Appl. Polym. Sci.* **2002**, *83*, 378.
[51] W. Lu, N. Jiang, J. Wang, *Adv. Mater.* **2017**, *29*, 1604862.
[52] L. Qi, M. Xiao, F. Wang, L. Wang, W. Ji, T. Man, A. Aldalbahi, M. Naziruddin Khan, G. Periyasami, M. Rahaman, A. Alrohaili, X. Qu, H. Pei, C. Wang, L. Li, *Nanoscale* **2017**, *9*, 14184.
[53] Y. Zhang, J. Yu, J. Wang, N. J. Hanne, Z. Cui, C. Qian, C. Wang, H. Xin, J. H. Cole, C. M. Gallippi, Y. Zhu, Z. Gu, *Adv. Mater.* **2017**, 29.
[54] J. Yu, Y. Zhang, Y. Ye, R. DiSanto, W. Sun, D. Ranson, F. S. Ligler, J. B. Buse, Z. Gu, *Proc. Natl. Acad. Sci. USA* **2015**, *112*, 8260.
[55] J. Yu, C. Qian, Y. Zhang, Z. Cui, Y. Zhu, Q. Shen, F. S. Ligler, J. B. Buse, Z. Gu, *Nano Lett.* **2017**, *17*, 733.
[56] H. Lee, T. K. Choi, Y. B. Lee, H. R. Cho, R. Ghaffari, L. Wang, H. J. Choi, T. D. Chung, N. Lu, T. Hyeon, S. H. Choi, D.-H. Kim, *Nat. Nanotechnol.* **2016**, *11*, 566.
[57] H. Lee, C. Song, Y. S. Hong, M. S. Kim, H. R. Cho, T. Kang, K. Shin, S. H. Choi, T. Hyeon, D.-H. Kim, *Sci. Adv.* **2017**, *3*, e1601314.
[58] N. Jiang, L. Shao, J. Wang, *Adv. Mater.* **2014**, *26*, 3282.
[59] X. Qu, M. Li, H. Zhang, C. Lin, F. Wang, M. Xiao, Y. Zhou, J. Shi, A. Aldalbahi, H. Pei, H. Chen, L. Li, *ACS Appl. Mater. Interfaces* **2017**, *9*, 31568.